Section 1
PROGRESS IN LASER FUSION

1.A Effect of Laser Illumination Nonuniformity on the Analysis of Time-Resolved X-Ray Measurements in UV Spherical Transport Experiments

Introduction

Thermal transport plays a key role in direct-drive laser fusion[1] because it affects the efficiency of the ablation process that drives the implosion of laser-driven targets. In transport experiments, the thermal electron flux is not measured directly but is inferred from measurable quantities. One such quantity is the burn-through rate of the heat front through a material that contains one or more x-ray-emitting signature layers.[2–6] Simulations are then carried out with a hydrodynamic code in which the thermal electron flux is characterized by the value of the flux limiter f required to replicate the experimental observations;[7] the flux limiter is the adjustable parameter in the definition of the free-streaming limit of the heat flux,

$$Q_f = f n_e (kT_e)^{3/2}/m_e,$$

which is the upper-limit on the heat flux. Experiments in spherical geometry have inferred various levels of flux inhibition, from as low as $f = 0.06$ with 1050-nm laser radiation,[3] to values of $f > 0.1$ at various laser wavelengths.[2,4,6] In all these experiments, the analysis of the measurements assumed that the laser intensity distribution on the target surface did not differ appreciably from the average intensity.

In a series of transport experiments conducted at LLE,[8] experimental results were such that the assumption of uniform laser intensity distribution could not hold any more. In these experiments, the

temporal dependence of the mass-ablation rate of spherical targets irradiated with UV-laser light was measured using time-resolved x-ray spectroscopy. The measured mass-ablation rate was found to be larger by a factor of 2 than that obtained in simulations with uninhibited heat flow, yet the scalings of the mass-ablation rate with absorbed intensity were in agreement. One of the reasons advanced for the discrepancy between experiment and simulation was that using only six beams of the OMEGA laser system at 351 nm produced a nonuniform illumination pattern on the targets.

The effect of laser illumination nonuniformity on the interpretation of thermal transport experiments has not been previously studied in detail. Yet, neglecting nonuniformity can lead to erroneous conclusions when the analyis of the thermal transport is based on spectroscopic diagnostics, which usually do not incorporate high spatial resolution. Nonuniformities in the multibeam illumination of spherical targets arise from two sources: nonuniformities in the individual beams and the result of the overlap of the individual beam distributions on the target surface.[9] The beam geometry and beam overlap lead to long-wavelength variations that have little effect on transport experiments. The nonuniformities that do affect the interpretation of transport experiments occur in the individual beams of the frequency-tripled OMEGA glass laser system and manifest themselves as small regions (< 20 μm in diameter in the target plane) of very high intensity, or "hot spots." If the hot spots contain a sufficiently large fraction of the total energy, their presence in the intensity distribution on the surface of the target can lead to the conclusion that the heat flux inferred from spectroscopic diagnostics is larger than would be obtained for a given nominal intensity. Such hot spots produce stronger line emission in the case of time-integrated burn-through experiments, or earlier emission in the case of time-resolved burn-through experiments, than expected from nominal intensity. This effect is more important for laser illumination at 351 nm than at 1060 nm because lateral thermal smoothing is not as effective at the shorter wavelength.[10] Illumination nonuniformity could also explain some of the discrepancies between results from various laboratories, since each laser system has its own distinctive illumination pattern resulting from differences in optics and beam quality.

In this report we present an analysis of recent time-resolved burn-through measurements on spherical targets and discuss the effect of illumination nonuniformities on the interpretation of the results. The analysis shows that taking into account the estimated level of nonuniformity of the laser illumination can advance the onset of the x-ray signature lines by about 100 ps and also affect the temporal shape of the line emission. Intensities larger than three times the nominal intensities were required to obtain agreement between the measured and computed onset times of signature lines. Also, the mass-ablation rate was measured for times past the peak of the pulse, when the rate had been predicted to drop rapidly.[8]

The measurements discussed in this report were part of a series of transport experiments carried out at 351 nm on the 24-beam OMEGA

laser system at LLE.[11] This system produces energies up to 2 kJ in approximately Gaussian-shaped pulses of about 600-ps (FWHM) duration. The laser beams are focused on the target in such a way as to provide the most uniform irradiation conditions.[12] The targets were solid glass spheres of two nominal diameters (300 μm and 600 μm), coated with 2 μm to 16 μm of parylene (CH) and suspended on submicron-diameter glass stalks. The nominal (average) intensities on target ranged from 3×10^{14} to 1×10^{15} W/cm^2.

The diagnostics included plasma calorimeters and charge collectors to characterize the absorption and the plasma blowoff, x-ray photography of the target, and time-resolved and time-integrated x-ray spectroscopy. In this report, emphasis is placed on time-resolved spectroscopic results obtained from the SPEAXS instrument,[13] in which an elliptically curved mica crystal analyzer was used to disperse the x-ray spectrum (1.5-keV to 3.2-keV range) onto the slit of an x-ray streak camera. The temporal characteristics of the burn-through were obtained by measuring the time of onset of the silicon Hβ line emission for targets with varying thicknesses of CH. A timing fiducial signal was generated by quadrupling the frequency of part of the main laser pulse obtained from mirror leakage and focusing it to a section of the photocathode consisting of a 200-Å layer of aluminum on mica.[14] The time of onset was defined as the time at which the intensity of a certain line emission exceeded the CH continuum emission by a factor of 2.

Details of the Analysis

The time-resolved spectra for two series of shots were digitized: one series at 3×10^{14} W/cm^2 with CH thicknesses of 0, 2, 4, and 6 μm, and the other at 1×10^{15} W/cm^2 with CH thicknesses of 0, 4, 8, and 12 μm. Superpositions of the digitized traces for the Si Hβ lines at each laser intensity are shown in Fig. 29.1. Time is measured relative to the peak of the laser pulse, as determined from the fiducial, and the vertical axis is the intensity of the line emission obtained from the measured *D*-log exposure curves for the streak camera recording film. The continuum emission was subtracted in order to obtain a clearly defined onset time. In marginal burn-through cases, such as for the 12-μm CH case in Fig. 29.1(b), the location of the onset of the line emission is difficult to determine from the lineout, but it can be clearly seen in the original photograph.

Simulations were performed with the one-dimensional Lagrangian hydrodynamic code *LILAC*,[15] which includes ray tracing, Thomas-Fermi equation of state, and multigroup diffusion radiation transport. The ray tracing is carried out using the azimuthally averaged spatial profile of a typical beam; the inverse-bremsstrahlung opacity is corrected for the Langdon effect.[16] The electron thermal energy was transported using a flux-limited diffusion model in which the effective flux was defined as the minimum of the diffusion flux and the free-streaming flux (the sharp-cutoff method). The opacities used in the radiation transport calculation were obtained from the Los Alamos LTE astrophysical library.[17] A finely resolved x-ray energy grouping was used in these simulations to provide a better treatment of the x-ray

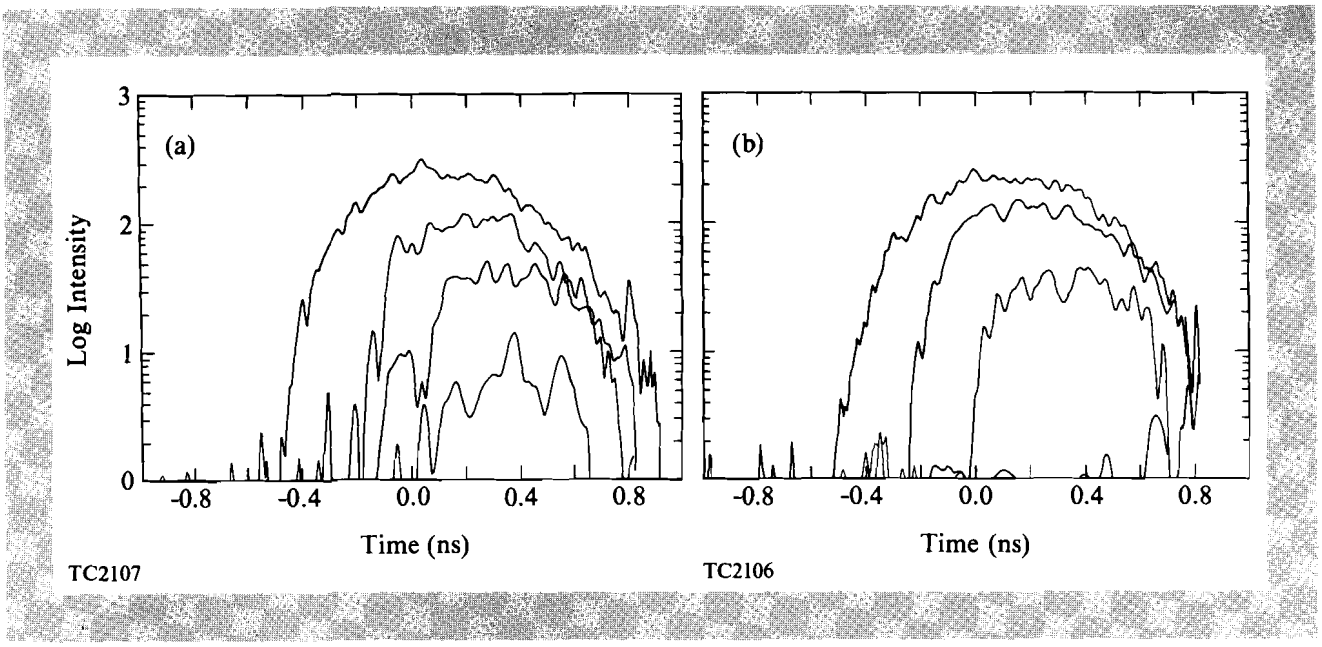

Fig. 29.1
Temporal emission of the Si Hβ line from SPEAXS:
(a) for 0, 2, 4, and 6 μm of CH over glass at 3×10^{14} W/cm^2;
(b) for 0, 4, 8, and 12 μm of CH at 1×10^{15} W/cm^2; the continuum has been subtracted.

line transport in the multigroup environment. The LTE line emissions presented in this report were obtained from the energy emitted from the narrow group (ΔE = 20 eV) that contained the Si Hβ line. Non-LTE considerations do not significantly affect the progress of the heat front through the low-Z plastic layer,[18] but may influence the onset of the silicon line emission. To appreciate this effect, the temporal line emission was also calculated with a non-LTE post-processor, which operates from *LILAC* results.[19]

To take into account the effect of the nonuniformity of the illumination of the target by a multibeam laser system, the overall laser intensity distribution on the target surface must be known. While it is not now possible to measure directly the intensity distribution at the target surface, one method of estimating this distribution is through the superposition of the equivalent-target-plane (ETP) intensity distributions of all the OMEGA laser beams. During this series of experiments, the illumination uniformity on target was estimated by using the measured two-dimensional ETP distribution from a single OMEGA beam as the input to a beam superposition code.[9] This code integrates the beam intensity distributions from all 24 beams of OMEGA, taking into account their position and orientation and the effects of refraction.[20] To approximate the differences between individual beam distributions, the two-dimensional ETP distribution was randomly oriented for different beams. The illumination uniformity is then characterized by decomposing the resulting spherical distribution into a histogram, shown in Fig. 29.2, which gives the relative energy in each intensity group on the target surface. The inset is a shaded contour plot of the target plane intensity distribution that was used. The plot contains several intensity hot spots about 15 μm to 20 μm across. The histogram shows a large peak at 1.4 times the nominal intensity I_0 (I_0 is the nominal intensity defined as the peak laser power divided by the initial target area) and residual energy at 1.9 I_0.

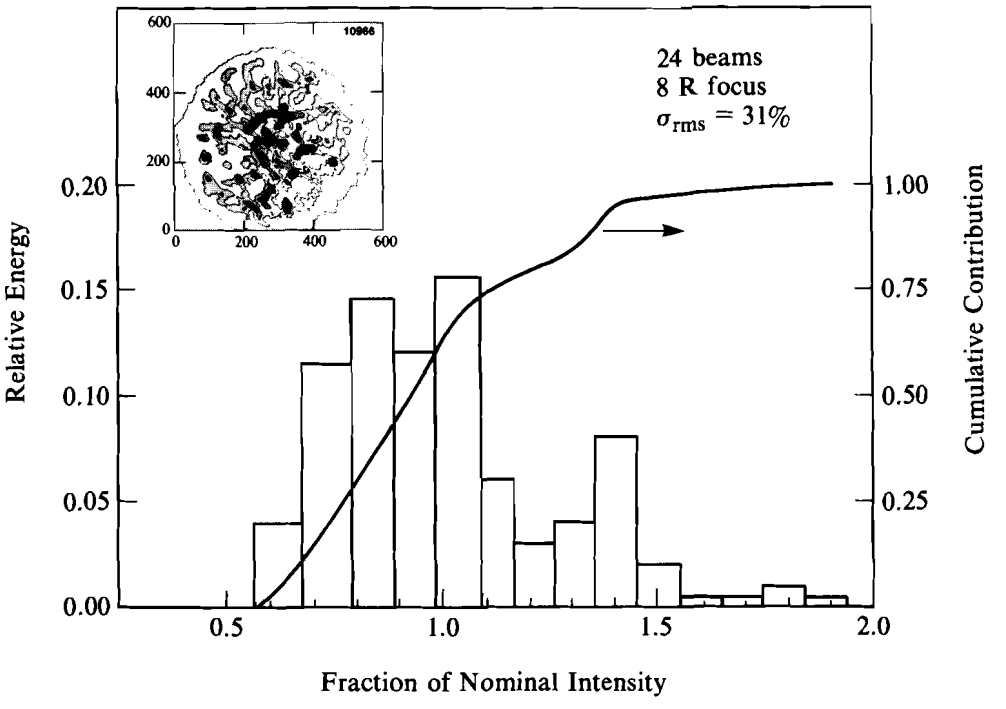

Fig. 29.2
Laser intensity variation on the target surface obtained from the equivalent-target-plane intensity distribution shown in the inset for 24 UV (351-nm) beams of OMEGA at 8-R (tangential) focus.

The distribution of intensities on target shown in Fig. 29.2 was used to estimate the temporal behavior of the x-ray line emission from the target in the presence of illumination nonuniformities. For a given target shot, *LILAC* simulations were performed for each of the 13 intensity distribution groups in Fig. 29.2. Each of these simulations produced a temporal emission of the silicon resonance lines (H- and He-like), which were then combined by weighting the emission for each intensity group by the fractional laser energy in that group.

Results of the Data Analysis

The first step in the simulations with *LILAC* was to adjust the flux limiter to agree at nominal intensity with the measured absorption fraction. This is in contrast with previous analyses of transport experiments[2–6] in which the goal had been to obtain agreement with the experimental transport data by varying the value of the flux limiter in the simulations; in most cases, agreement with the measured absorption fraction was not sought. This is not the goal in the present analysis. The absorption fraction was used to adjust the flux limiter because it is an integrated measurement that depends weakly on the intensity distribution. This weak dependence was verified by comparing the absorption fraction for a simulation at nominal intensity to the weighted-average absorption fraction: the relative difference in the absorption fraction was less than 10%. The flux limiter value of 0.06 (sharp cutoff) was used in all simulations unless otherwise noted.

The weighted-average temporal emissions for the Si Hβ line for the cases of Fig. 29.1 are shown in Fig. 29.3. The arrows denote the measured onset times obtained from the traces in Fig. 29.1. The weighted-average onset times are the same as those calculated for 1.4 I_0 because a significant amount of energy is present at that intensity (see Fig. 29.2). For all plastic thicknesses, the calculated onset times lag the measured times. In both series, the lag increases from about 100 ps for the smallest plastic thickness (excluding zero thickness) to 200 ps for the second thickness. For the largest thicknesses of plastic, which are marginal burn-through cases, the computed line emission is either nonexistent (12 μm in the high-intensity case) or much weaker than the measured line emission (6 μm in the low-intensity case). The effect of varying the flux limiter is illustrated in Fig. 29.4, where the temporal emission for a single thickness of plastic (4 μm at 3×10^{14} W/cm^2 and 8 μm at 1×10^{15} W/cm^2) is plotted at nominal laser intensity for increasing values of the flux limiter. The measured onset times are now denoted by shaded band with an estimated absolute error of ±50 ps. At 3×10^{14} W/cm^2, increasing the flux limiter to 0.08 decreases the onset time by only about 50 ps; further increasing the flux limiter has no effect. In this case, it is not possible to simulate correctly the measured onset time even with unrestricted Spitzer heat flow. At 1×10^{15} W/cm^2, the onset time is more sensitive to the flux limiter, but again, heat fluxes larger than classical Spitzer fluxes would be required to simulate the measured temporal line emission. Therefore, the experimental results can only be explained by the presence of significant energy in the laser intensity distribution at intensities larger than 1.5 I_0.

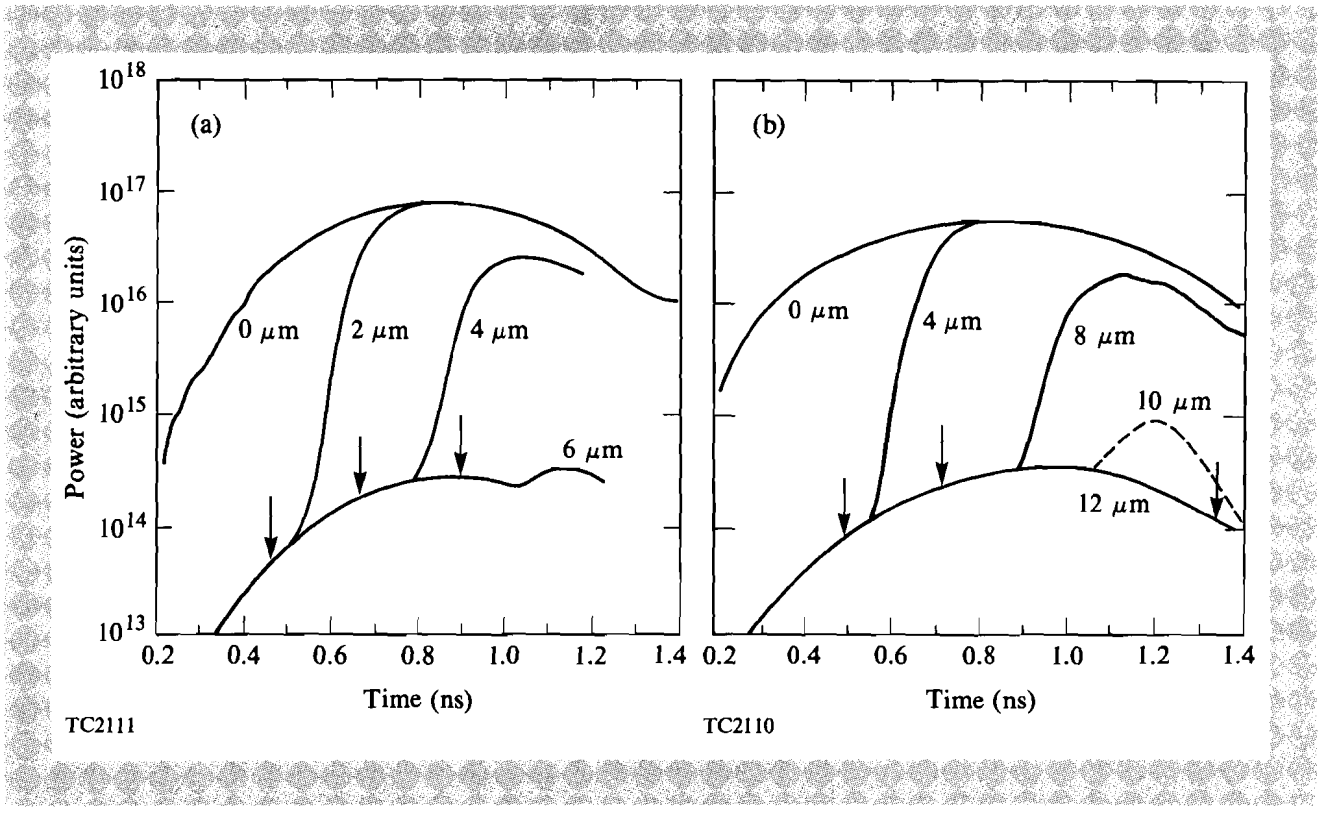

Fig. 29.3
Weighted-average temporal Si Hβ emission from *LILAC* calculated from the intensity distribution in Fig. 29.2:
(a) 3×10^{14} W/cm^2; and
(b) 1×10^{15} W/cm^2.
Arrows indicate the experimental times.

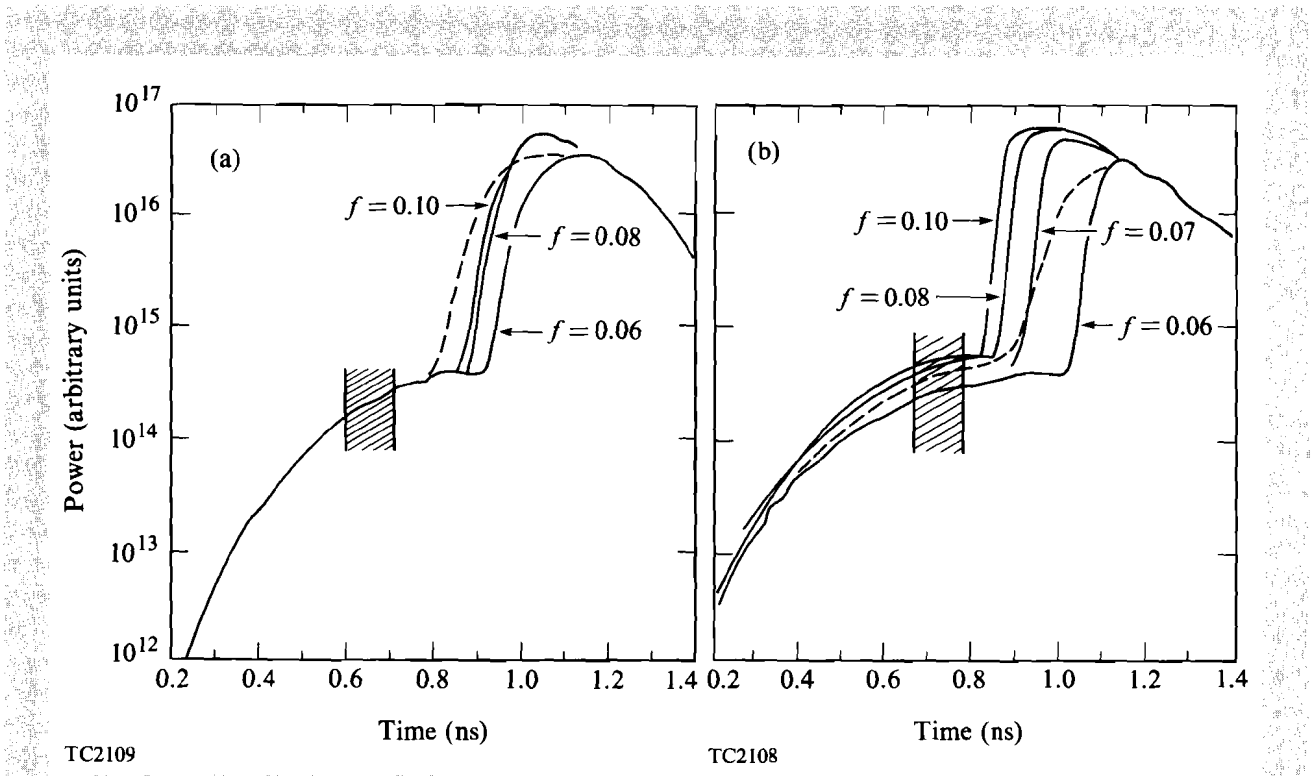

Fig. 29.4
Effect of varying the flux limiter on the onset of line emission and comparison between line emission at nominal intensity (solid lines) and the weighted-average line emission (dashed line):
(a) 3×10^{14} W/cm^2; and
(b) 1×10^{15} W/cm^2.

Based on the conclusion of Ref. 8—that absorbed intensities three times nominal would be required to match the measured mass-ablation rates with $f = 0.1$ (harmonic)—simulations were carried out for the two series of shots with incident intensities up to 3 I_0. The effect of varying the laser intensity from about 0.5 I_0 to 3 I_0 on the onset time of the Si Hβ line is shown in Fig. 29.5, where the onset time relative to the peak of the pulse is plotted as a function of the laser intensity on target normalized to the nominal intensity. The shaded bands represent the measured onset time with an estimated absolute error of ± 50 ps. In Figs. 29.5(a) and 29.5(b), for the case of the thinnest CH thickness, the heat front burns through to the glass for intensities below 0.6 I_0. For larger thicknesses of CH, line emission is produced only above a certain threshold intensity. Except for the two points nearest to the threshold intensity, the onset time scales as the laser intensity to some power that is different for each plastic thickness; the values of that power scaling range from 0.2 to 0.4. In Fig. 29.5, the onset times at 1.4 I_0 reflect the same lag with respect to the measured onset times, as seen in Fig. 29.3. For the series at 3×10^{14} W/cm^2, the calculated onset time at 3 I_0 agrees well with the experimental values for the three plastic thicknesses. This agreement, coupled with the fact that the onset times are not very sensitive to flux limiter values above 0.06, strongly suggests that some fraction of the incident laser energy must reside at intensities on target near 3 I_0 in the form of small, intense hot spots. At 1×10^{15} W/cm^2, agreement is obtained for 4 μm and 8 μm of plastic. For the 12-μm plastic case, the computed time is now about 200 ps ahead of the measured time. Attempts to increase that time further would result in the disappearance of the line emission, as

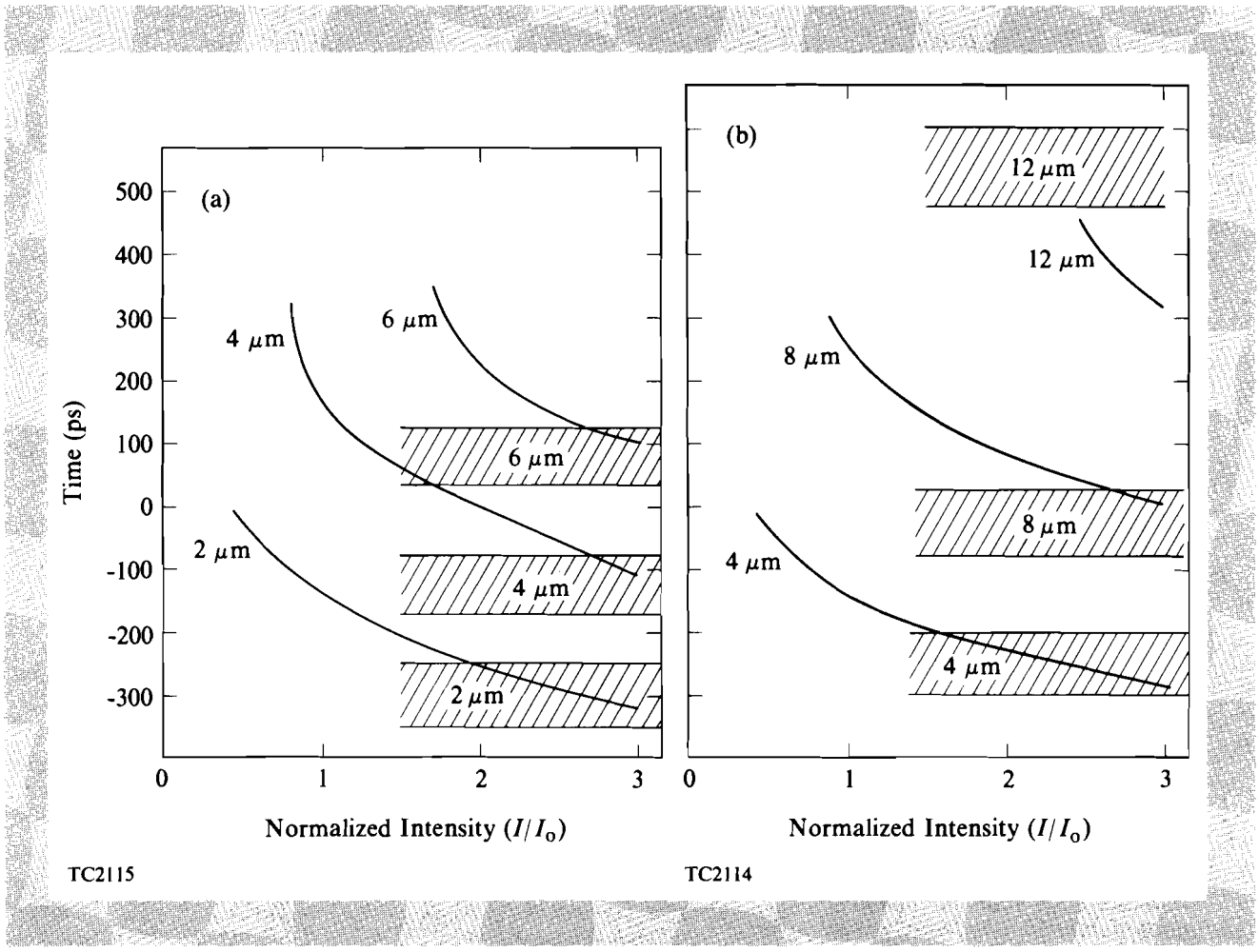

Fig. 29.5
Calculated onset times for the Si Hβ line as a function of the laser incident intensity; the shaded bands are the measured onset times and their uncertainty:
(a) 3×10^{14} W/cm^2; and
(b) 1×10^{15} W/cm^2.

can be seen in Fig. 29.5(b). The difficulty may lie in the fact that the onset time may not be known accurately because the burn-through is marginal at that plastic thickness. The argument that three times nominal intensity is required to explain the experimental results is not as straightforward at 1×10^{15} W/cm^2 as at 3×10^{14} W/cm^2, because the onset time is more sensitive to the flux limiter at the higher laser intensity; higher intensities and higher flux limiters are interchangeable in producing earlier onset times. Taken together, however, the analyses of the two series of shots strongly suggest that there is significant energy at 3 I_0 on the target surface.

It is difficult to estimate the fraction of the energy present in the laser intensity distribution above 1.5 I_0. One way is to consider the sensitivity of SPEAXS, which can be estimated experimentally from the amount of absorbed energy needed to observe the onset of the Si x-ray line emission: about 2% of the total absorbed energy (20 J to 30 J). But this is the amount of energy required to observe a signal above the noise level. The quantity of interest is the amount of energy that leads to an observable change in the onset time of the x-ray lines. This quantity could be estimated theoretically by modifying the laser intensity distribution of Fig. 29.2. The difficulty lies in how to distribute the additional energy above 1.5 I_0. Adding energy near

1.5 I_0 has less of an effect than adding the same amount of energy at 3 I_0. This is because, near 1.5 I_0, the increased emission is so close to the onset of the line emission from the known intensity distribution (Fig. 29.2) that it is added to the existing line emission rather than to the continuum emission, ahead of the onset, as is the case at 3 I_0. Because the actual laser intensity distribution between 1.5 I_0 and 3 I_0 is probably continuous, but not necessarily monotonically decreasing, it is not possible to get a precise estimate from theoretical considerations of the energy present in that intensity range. Reasonable estimates based on adding energy at 1.5 I_0 and 3 I_0 place this value at between 2% and 5% of the incident laser energy.

The method used in this report to estimate the effect of laser illumination nonuniformity on the interpretation of transport experiments has several limitations, one of which is that it does not include the effect of thermal smoothing. However, theoretical studies[10] indicate that lateral heat flow contributes little to thermal smoothing for nanosecond-duration 351-nm pulses on spherical targets. Another possible limitation arises from the fact that the illumination was estimated with the distribution of only a single beam of OMEGA rather than with those of all 24 beams. The quality of the frequency tripling cells varies from beam to beam. The single-beam-laser intensity distribution used in the calculation of the intensity distribution on the target surface was obtained for a beam produced by a crystal cell of average quality, not by the worst one. Finally, because the spatial resolution of the ETP distribution was limited to about 20 μm, the hot spots may be smaller than 20 μm and their intensity could possibly be larger than presently measured. Consideration of these limitations leads to the conclusion that the actual intensity distribution on target probably contains a larger fraction of the laser energy at the high intensities than in the estimated intensity distribution shown in Fig. 29.2.

Effect of Illumination Uniformity

Fig. 29.4 illustrates how including the illumination nonuniformity in the analysis of time-resolved spectroscopic measurements can affect conclusions regarding the thermal transport. This is seen by comparing onset times from nominal intensity simulations for varying values of the flux limiter with the weighted-average times. In Fig. 29.4(a), no values of the flux limiter will give the same onset time as the weighted-average onset time because the thermal transport is not sensitive to the flux limiter for $f > 0.08$. At 1×10^{15} W/cm^2, the weighted-average onset time is obtained for $f = 0.07$, not very different from the nominal value of $f = 0.06$. It should be noted that part of the change in the onset time is also due to the increase in the absorption fraction associated with the increase in the flux limiter. An immediate conclusion is that, in order to match computed onset times to measured onset times, simulations with nominal intensity would yield larger values of the flux limiter than would be obtained when illumination nonuniformities are included; in fact, at low intensity, the heat flux would have to be larger than classical heat flux to match the measured onset times. The inclusion of illumination nonuniformity in the simulations also results in the presence of line emission that would

not be produced at the nominal intensity: for example, at 3×10^{14} W/cm^2 and 6 μm of CH, line emission occurs only for laser intensities above 1.5 I_0. Another effect of including the illumination nonuniformity arises from the fact that the onset times are different for each of the illumination intensities on the target. While the rise time from the simulations at individual intensities is very steep, typically less than 50 ps (see Fig. 29.4), the weighted-average emission has a slower rise time—longer than 100 ps. This is because the various illumination intensities contribute to the emission rise at different times. Thus, x-ray emission rise times, which are large in the experiment (see Fig. 29.1), are sensitive to the illumination uniformity: more uniform illumination will lead to steeper rise time.

The onset of the calculated x-ray line emission and its rise times can also be affected by the inclusion of non-LTE atomic physics in the simulation. Because non-LTE ionization lags behind LTE ionization, one can expect the emission onset to occur later and the rise time to be longer for the non-LTE case. Simulations that included non-LTE post processing resulted in small differences in the line-emission onset time. In Fig. 29.6 are plotted the LTE and the non-LTE temporal line emission for a given plastic thickness at both laser intensities. At 3×10^{14} W/cm^2, the non-LTE onset time lags the LTE time by about 50 ps–70 ps; at 1×10^{15} W/cm^2, there is no lag. It is not obvious why there should be a difference between the two cases. The other differences observed were a longer rise time for the non-LTE

Fig. 29.6
Comparison between LTE (solid line) and non-LTE (dashed line) line emission for Si Hβ:
(a) 4 μm of CH at 3×10^{14} W/cm^2; and
(b) 8 μm of CH at 1×10^{15} W/cm^2.

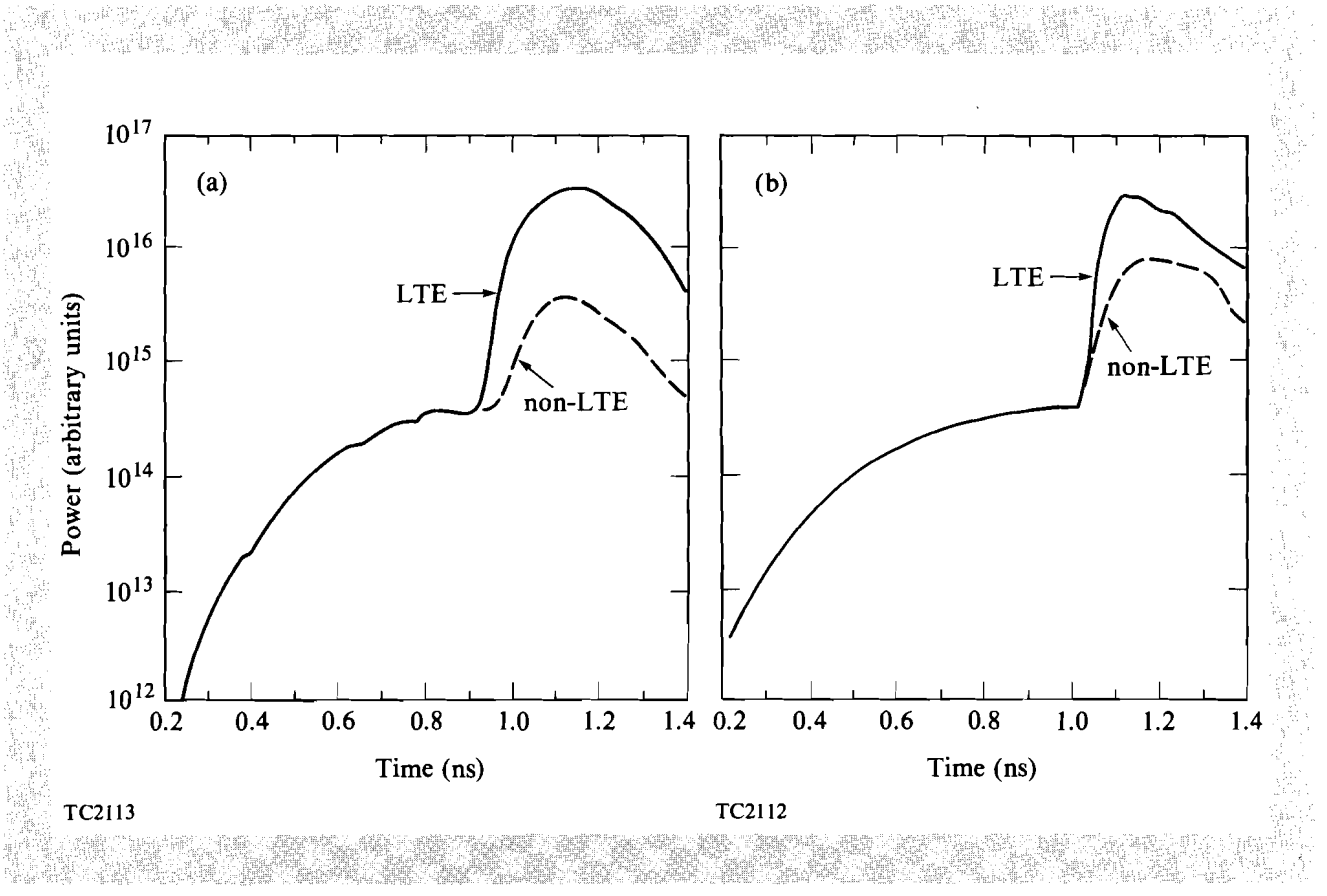

emission and a lack of line emission for marginal burn-through cases, such as 8 μm of CH at 3 $\times$ 10^{14} W/cm^2. The increase in rise time due to non-LTE is not large enough to explain the long rise times observed experimentally.

The aim of burn-through experiments is to measure the mass-ablation rate, which is an indication of the efficiency of the drive. The instantaneous mass-ablation rate is calculated[8] at the temporal midpoint between the onset of line emission at two plastic thicknesses using $\dot{m} = \rho\Delta d/\Delta t$, where ρ is the density of solid CH, Δd is the difference in the CH thicknesses, and Δt is the difference in onset time. If the target were uniformly illuminated, such an analysis would give the actual drive mass-ablation rate. But when the illumination contains high-intensity hot spots, burn-through measurements yield unreasonably large values for the mass-ablation rate because the onset time of the line emission corresponds to that of the high-intensity hot spots.[8] Therefore, while the absolute value of the measured mass-ablation rate reflects the level of nonuniformity, what is of interest is the scaling of the mass-ablation rate with absorbed intensity and how it compares with simulation. The mass-ablation rate is obtained from *LILAC* simulations by following the temporal excursion of the 500-eV isotherm (500 eV is approximately the temperature required for Si Hβ line emission). In this case, the same expression is used for calculating the mass-ablation rate except that now, Δd is the excursion of the 500-eV isotherm during the interval Δt. Several sets of mass-ablation rates are plotted against the absorbed intensity in Fig. 29.7. The discrete points are the instantaneous mass-ablation rate as calculated from the onset of line emission from experiment (solid symbols), from the weighted-average analysis (open symbols with cross), and from simulations at 3 I_0 (open symbols). The squares were obtained from the series at 3 $\times$ 10^{14} W/cm^2 and the circles from the series at 1 $\times$ 10^{15} W/cm^2. The solid line describes the computed mass-ablation rate from the 500-eV isotherm excursion from simulation at 3 I_0. The

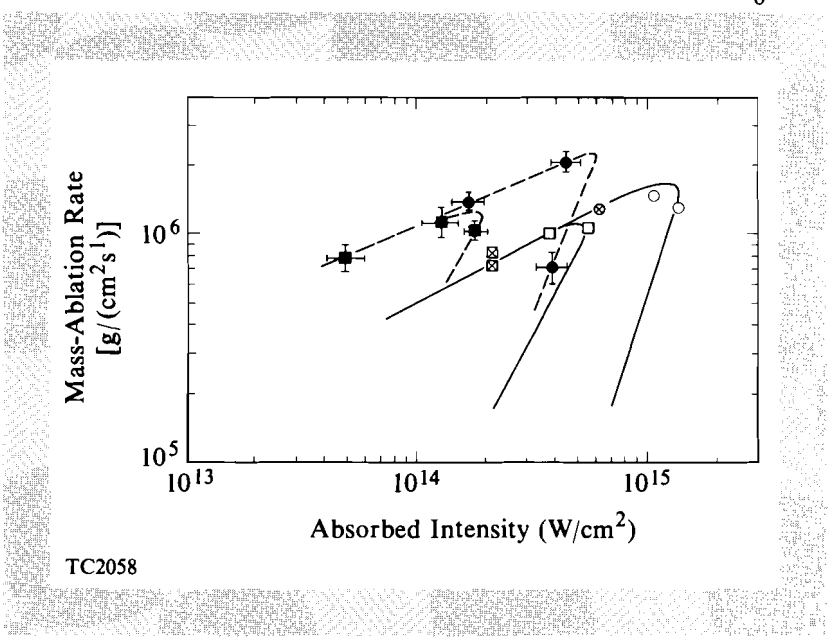

Fig. 29.7
Comparison between the instantaneous mass-ablation rate from experiment and simulation. The solid line is obtained from the excursion of the 500-eV isotherm in simulations at 3 I_0. The points are calculated from the onset times of the Si Hβ line; the dashed lines have been added for clarity. Squares are at 3 $\times$ 10^{14} W/cm^2 and circles at 1 $\times$ 10^{15} W/cm^2; solid: experiment; open: simulation at 3 I_0; cross: simulation, weighted average.

dashed line has been added to show how the discrete points belong to two sets of instantaneous mass-ablation-rate curves that parallel the set of simulation curves. On these curves, the peak of the pulse occurs in the middle of the "elbow." For the experimental points, the absorbed intensity was obtained from code simulation at nominal intensity.

The two experimental points on the downside of the dash curve confirm the rapid decrease of the mass-ablation rate, which had been predicted to occur after the peak of the pulse.[8] A scaling of the mass-ablation rate with absorbed intensity was obtained from the rising dash line: $\dot{m} \propto I^{0.43}$; the solid curve shows a slightly different scaling from simulation: $\dot{m} \propto I^{0.53}$. These scaling laws, but not the magnitude, are in reasonable agreement with those derived in Ref. 6 from charge collector data. Both the scaling and the magnitude of the mass-ablation rate are comparable to those obtained in the six-beam experiments.[8] Since the weighted-average points at 3×10^{14} W/cm^2 bracket the peak of the pulse and are very close, their value must be near to the maximum value of the weighted-average mass-ablation rate; this maximum mass-ablation rate is about two thirds of the measured value. Only the mass-ablation rate obtained from simulations at 3 I_0 approaches the experimental value; even there, the peak values from simulation are slightly lower than the measured values.

Summary

Transport experiments were carried out on the 24-beam OMEGA laser system at 351 nm. The laser beams were focused on spherical signature targets (glass balls or thick glass shells coated with CH) in such a way as to maximize the illumination uniformity. The temporal progress of the heat front was measured absolutely with the time-resolved x-ray spectrometer SPEAXS. Simulations of the experiment were carried out by taking account of the nonuniformity of the laser illumination on the target surface. The 24-beam illumination was characterized by superposing the ETP intensity distribution from one beam of OMEGA over the target surface. Weighted-average temporal profile of the line emissions was calculated from *LILAC* simulations at the intensities characterizing the intensity distribution on target. Inclusion of the nonuniformity advanced the onset time of the Si Hβ line by about 100 ps over the time calculated with the nominal intensity. But this advance in onset time was not sufficient to obtain agreement with the measured onset time. Increasing the value of the flux limiter from 0.06 to 0.1 made little difference at 3×10^{14} W/cm^2 and not enough at 1×10^{15} W/cm^2. The simulation intensities had to be increased to 3 I_0 for the onset times to agree with the experiment, suggesting that significant energy (a few percent) must exist at intensities equal to or larger than three times nominal.

The results of the transport experiment and their interpretation, using simulations that included the effects of illumination nonuniformity, lead to the following conclusions:

1. The effects of illumination nonuniformity cannot be neglected in the interpretation of transport experiments in which the progress of the heat front is measured spectroscopically, both in the time-resolved and time-integrated modes. Since the onset of

x-ray line emission or the burn-through depth can be affected by varying either the flux limiter or the laser intensity distribution on target, a full knowledge of the laser intensity distribution at the target surface would be required to pin down the value of the flux limiter using burn-through diagnostics. If the presence of illumination nonuniformity were neglected, a larger value of the flux limiter would be inferred than if illumination nonuniformity were taken into account.

2. The steep falloff of the scaling of the mass-ablation rate with absorbed intensity, observed in *LILAC* simulations,[8] has been confirmed experimentally. This result indicates that a single scaling cannot be used throughout the laser pulse in the interpretation of time-integrated measurements.

3. In the present experiments, the effect of non-LTE is small; it retards the onset of the x-ray line emission by at most 50 ps and increases slightly the rise time of that emission.

4. To obtain estimates of the mass-ablation rate in the presence of illumination nonuniformity, it is necessary to use diagnostics that are sensitive to the integrated or averaged intensity distribution on target. Such diagnostics include measurements of the ion blowoff distribution and of the implosion time. X-ray diagnostics of burn-through will be a useful diagnostics when the illumination uniformity is improved (for example, through the use of better optics or of incoherent illumination) or with the use of targets with high-Z dots imbedded in the plastic ablator (assuming that the intensity hot spots are not smaller than the dots).

5. X-ray diagnostics of targets with signature layers turn out to be good diagnostics of the illumination uniformity.

ACKNOWLEDGMENT

This experiment was part of a joint series of experiments with the Lawrence Berkeley National Laboratory, the Los Alamos National Laboratory, and the University of Maryland. The work at the University of Rochester was supported by the U.S. Department of Energy Office of Inertial Fusion under agreement No. DE-FC08-85DP40200 and by the Laser Fusion Feasibility Project at the Laboratory for Laser Energetics, which has the following sponsors: Empire State Electric Energy Research Corporation, General Electric Company, New York State Energy Research and Development Authority, Ontario Hydro, and the University of Rochester. Such support does not imply endorsement of the content by any of the above parties.

REFERENCES

1. J. Nuckolls, L. Wood, A. Thiessen, and G. Zimmerman, *Nature* **239**, 139 (1972).

2. T. J. Goldsack, J. D. Kilkenny, B. J. MacGowan, P. F. Cunningham, C. L. S. Lewis, M. H. Key, and P. T. Rumsby, *Phys. Fluids* **25**, 1634 (1982).

3. J. A. Tarvin, W. B. Fechner, J. T. Larsen, P. D. Rockett, and D. C. Slater, *Phys. Rev. Lett.* **51**, 1355 (1983).

4. B. Yaakobi *et al.*, *Phys. Fluids* **27**, 516 (1984).

5. A. Hauer *et al.*, *Phys. Rev. Lett.* **53**, 2563 (1984).

6. B. Yaakobi *et al.*, *J. Appl. Phys.* **57**, 4354 (1985).

7. R. C. Malone, R. L. McCrory, and R. L. Morse, *Phys. Rev. Lett.* **34**, 721 (1975).

8. P. A. Jaanimagi, J. Delettrez, B. L. Henke, and M. C. Richardson, *Phys. Rev. A* **34**, 1322 (1986).

9. S. Skupsky and K. Lee, *J. Appl. Phys.* **54**, 3662 (1983).

10. S. E. Bodner, *J. Fusion Energy* **1**, 221 (1981); J. H. Gardner and S. E. Bodner, *Phys. Rev. Lett.* **47**, 1137 (1981).

11. J. M. Soures, R. J. Hutchison, S. D. Jacobs, L. D. Lund, R. L. McCrory, and M. C. Richardson, in the *Proceedings of the Tenth Symposium on Fusion Engineering*, Philadelphia, PA (1983), p. 1392.

12. M. C. Richardson, P. W. McKenty, F. J. Marshall, C. P. Verdon, J. M. Soures, R. L. McCrory, O. Barnouin, R. S. Craxton, J. Delettrez, R. L. Hutchison, P. A. Jaaminagi, R. Keck, T. Kessler, H. Kim, S. A. Letzring, D. M. Roback, W. Seka, S. Skupsky, B. Yaakobi, and S. M. Lane, in *Laser Interaction and Related Plasma Phenomena Vol. 7,* edited by H. Hora and G. Miley (Plenum Press, New York, 1986).

13. B. L. Henke and P. A. Jaanimagi, *Rev. Sci. Instrum.* **54**, 1311 (1983).

14. P. A. Jaanimagi, L. DaSilva, G. G. Gregory, C. Hestdalen, C. D. Kiikka, R. Kotmel, and M. C. Richardson, *Rev. Sci. Instrum.* **57**, 2189 (1986).

15. An earlier version of *LILAC* is described in Laboratory for Laser Energetics Report No. 16 (1976).

16. A. B. Langdon, *Phys. Rev. Lett.* **44**, 575 (1980).

17. W. F. Huebner, A. L. Merts, N. H. Magee, and M. F. Argo, Los Alamos Report No. LA-6760 (1977).

18. Recent simulations, in which a non-LTE atomic physics model was included directly into *LILAC* (rather than as a postprocessor), showed little difference in the progress of the heat front in CH when compared to LTE results.

19. R. Epstein, S. Skupsky, and J. Delettrez, *J. Quant. Spectrosc. Radiat. Transfer* **35**, 131 (1986).

20. M. C. Richardson, S. Skupsky, J. Kelly, L. Iwan, R. Hutchison, R. Keck, R. L. McCrory, and J. M. Soures, *Proceedings of the 1983 Los Alamos Conference on Optics* (SPIE, Bellingham, WA, 1983), Vol. 380, p. 473.